We are IntechOpen,
the world's leading publisher of
Open Access books
Built by scientists, for scientists

6,900
Open access books available

185,000
International authors and editors

200M
Downloads

154
Countries delivered to

Our authors are among the

TOP 1%
most cited scientists

12.2%
Contributors from top 500 universities

BOOK CITATION INDEX
CLARIVATE ANALYTICS
INDEXED

WEB OF SCIENCE™

Selection of our books indexed in the Book Citation Index
in Web of Science™ Core Collection (BKCI)

Interested in publishing with us?
Contact book.department@intechopen.com

Numbers displayed above are based on latest data collected.
For more information visit www.intechopen.com

Application of Knudsen Force for Development of Modern Micro Gas Sensors

Mostafa Barzegar Gerdroodbary

Abstract

Development of new simple gas sensor is highly significant due to its various industrial applications. In this chapter, comprehensive studies on the new micro gas sensor of Micro In-plane Knudsen Radiometric Actuator (MIKRA) are done to evaluate the performance of its technique on the detection of gas. This new micro gas sensor works by the radiometric phenomena, which occurs due to temperature difference in rarefied gas. In order to simulate this micro gas sensor, direct simulation Mont Carlo (DSMC) is recognized as a reliable method. This study highly focused on the main mechanisms of the flow feature and force generation in low-pressure domain. In order to study this micro gas sensor, comprehensive numerical results are thoroughly investigated and the effects of primary factors and parameters are revealed. In addition, the main details of computational approach for the simulation of this micro gas sensor are fully presented. Finally, the performance of this sensor in various operating conditions is explained and main findings are discussed.

Keywords: micro gas sensor, Knudsen force, rarefied gas, DSMC

1. Introduction

Gas sensors are widely used in various industrial applications for evaluation of the main elements inside the gas mixture. In addition, this device is significant for detection of dangerous gas such as CO_2, H_2 and ammonia. In addition, gas sensors are widely used for the evaluation of the main products of the combustion. Since this instrument is a main element in the various applications, considerable researches and studies have been performed to develop new techniques for the detection of the various gases. Indeed, the present gas sensor is highly expensive and spacious and these disadvantages of the current sensors have motivated the researchers to develop a simple and cheap method for the gas detection [1–6].

Various methods and techniques are applied for the gas sensors [7–10]. However, current sensors could not perform in the micro scale. Recently, scientists and researchers have investigated molecular force which is produced by the temperature difference on the solid body in high Knudsen numbers. Since this force occurs in high Knudsen numbers, it is known as Knudsen force.

Knudsen number (Eq. (1)) is mainly defined as the ratio of the mean free path of gas (λ) to specific length (L) as follows:

$$Kn = \frac{\lambda}{L} = \frac{\mu}{p_\infty L}\sqrt{\frac{2\,k_B T_\infty}{m}}. \tag{1}$$

In Eq. (1), the term of mean free path of gas (λ) is proportional to the temperature and viscosity. According to this equation, high Knudsen number is obtained by decreasing either the pressure of the domain or size of our model. Previous studies [8–16] clearly showed that the Knudsen force is highly proportional to the main characteristics of the gas inside the domain.

Actually, thermal stresses are produced by the non-uniformity of the temperature within rarefied gases and create bulk fluid flows that could employ forces on solid body [17, 18]. Ketsdever et al. [17] presented broad literature reviews to reveal the origin of the Knudsen thermal force. They widely considered the technical remark of source of the Knudsen thermal force and active factor on the rate of induced forced. According to their findings, operative factors such as pressure of domain and gas component as well as the thermal gradient magnitude play significant role on the value of the exerted force. These characteristics enable researchers to apply this for the measurement of gas type.

One of the effective methods to apply the Knudsen force is to reduce the size of the model and construct micro device [19]. Micro Knudsen gauge and microscale radiometric actuator are the main conventional devices that implement this technique for industrialized applications. Numerous studies have been directed to inspect and evaluate the key features of Knudsen force in these instruments [18]. Strongrich et al. [19] performed experimental work and numerical studies to calculate Knudsen force on a non-uniformly heated beam. They highly focused on this molecular force and finally offer their new micro gas sensor as Micro In-plane Knudsen Radiometric Actuator (MIKRA) as shown in **Figure 1**. This sensor could be used either detection of gas types or measurement of gauge pressure [20, 21]. One of the significant aspects of this micro gas sensor is the micro size of this device that enables it to work in the various operating condition. Since this device is highly significant, considerable works have been performed to evaluate this micro gas sensor [11–13]. In our these papers, the main characteristics of this sensor are investigated and the precision of measured Knudsen force for different gas mixtures, for instance, hydrogen, methane/helium, methane/SO_2, carbon dioxide, ammonia, and inert gas. These researches are conducted to reveal the performance and capability of this micro gas sensor in diverse operating conditions [14–18]. These works have
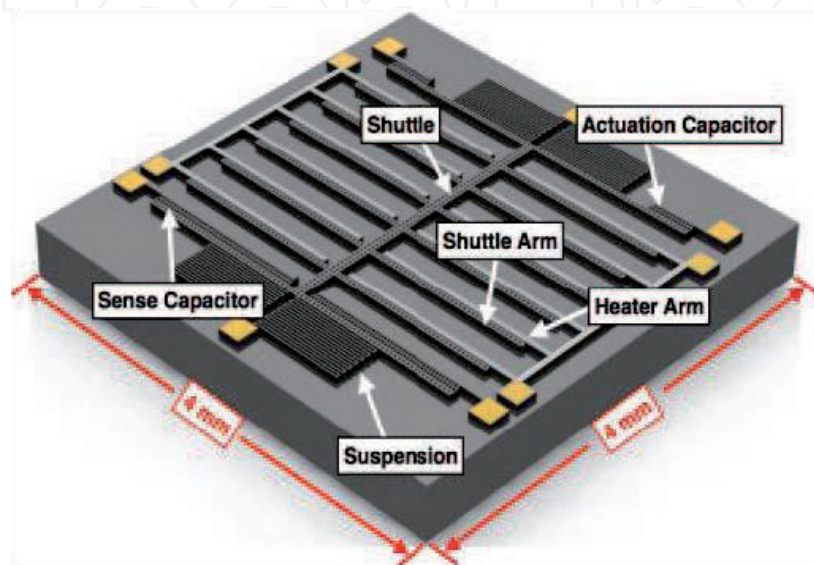

Figure 1.
Micro In-plane Knudsen Radiometric Actuator (MIKRA) [21].

tried to disclose the influence of temperature difference of cold and hot arm, the gap size, and pressure of domain on the value of the exerted force on the cold side.

The physics of the Knudsen force in the Knudsen gage are widely investigated by the researchers and scholars. Passian et al. [22–24] as pioneer research group initiated to reveal the main characteristic of the Knudsen force at the microscale. They mainly studied on a micro cantilever which includes two surfaces with dissimilar temperatures separated by a gap in rarefied domain. Theoretical and experimental studies have been conducted via a U-shaped silicon microcantilever to disclose the main parameters. The impact of thermal difference on the Knudsen forces in the transitional regime is examined by Lereu et al. [25]. The measurement of these forces at ordinary environment on test configurations made by surface micromachining of polysilicon are done by Sista and Bhattacharya [26]. Kaajakari and Lal [27] studied Knudsen forces produced within molecular flow regime to examine surface micromachined hinged structure assembly. Furthermore, negative thermophoretic force is studied by different scholars [28] and the influence of valuable factors on radiometric force is disclosed [29, 30].

In order to simulate the model, DSMC approach is a reliable technique for evaluation of the exerted Knudsen force in the rarefied domain. This method is highly popular and conventional for the simulation of the problems with low-pressure condition. Hence, numerous scholars and scientists [31–40] applied this for the simulation of scientific and engineering problems.

Recognition of the force value in the low-pressure domain is the primary challenge in this field. Indeed, scholars have performed various studies to obtain the reliable and comprehensive correlation which offers the main value of Knudsen force in various operating and geometrical conditions [41–46]. Following the above description and containing the historical perspective, the broadly established modern appreciative is such that the major force related to vane rotation is the force generated close to the edges of the vane, in a zone with the dimensions of a mean free path according to Einstein. At very low pressures, the mean free path is great and the entire area of the vane is involved in force generation. As the pressure rises and flow enters the transition regime, the mean free path shrinks and the effective force-producing area of the vane is reduced. At some pressure (where the free path is on the order of the vane thickness according to Einstein), a maximum is gotten and force generation thereafter initiates to weaken as thermal creep and then convective currents initiate to lead the flow. A brief visual summary of the expected force output of a Nichols radiometer vane in free-space is shown in **Figure 2**, where comparisons are made for several of the dominant theories of the previous century. Here, FM denotes free molecular, B&L denotes Brüche and Littwin experimental measurements and "Einstein" denotes his correlation.

For a Crookes type radiometer, Scandurra et al. [46] have offered a first expression for radiometric force that includes both pressure and shear components. For the normal force per unit area (pressure difference) on a thin vane, they offered

$$F_n = (2 - \alpha_E) \frac{15\,k}{32\,\sqrt{2}\,\pi\sigma^2}\,\Delta T l, \tag{2}$$

where α_E is the energy accommodation coefficient, k is the Boltzmann constant, $\pi\sigma^2$ is the total collision cross section of the gas molecule, and l is the vane perimeter. For the shear stress, the expression is

$$F_\tau = \alpha_E \frac{15\,k}{64\,\sqrt{2}\,\pi\sigma^2}\,\frac{\Delta T}{\lambda}(\tau l), \tag{3}$$

where τ is the vane thickness. One of the key assumptions of that work is constant pressure in the gas surrounding the heated vane.
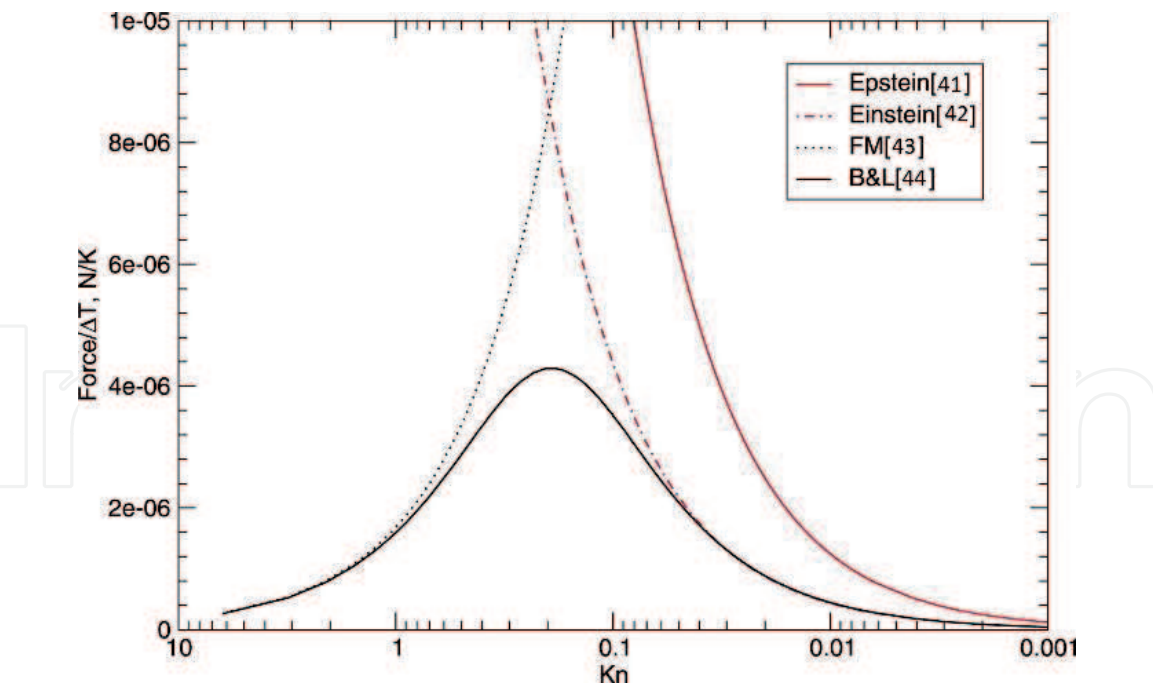
Figure 2.
Nichols radiometer: force prediction.

For a Crookes radiometer, practically, all earlier analytical estimates of the radiometric force, with the exception of the Brüche and Littwin bell-shaped correlation, were implicitly or explicitly assuming a collision-dominated flow, where the radiometer vane area is much larger than the gas mean free path. This is essentially a slip flow regime, where the impacts of the free molecular, area-related forces are relatively small. This explains that the proposed expressions depend on the perimeter of the radiometer vane, and not on its area. While this is a reasonable approach for many cases, where the velocity distribution function is close
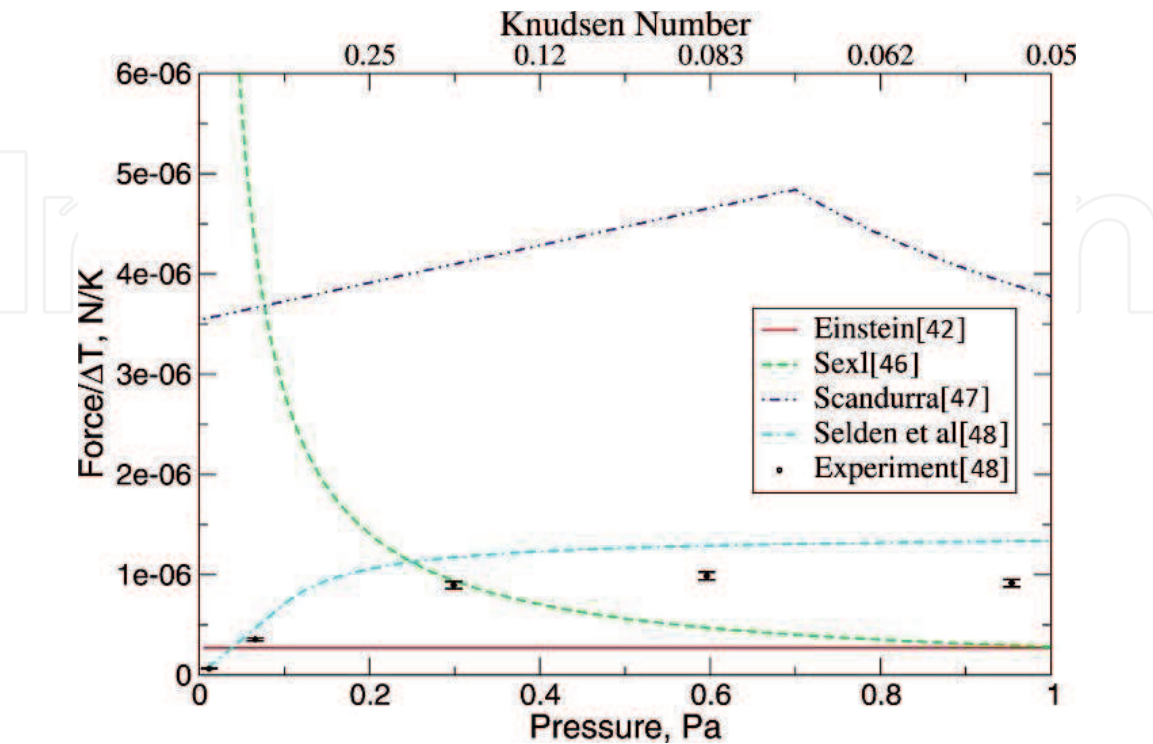

Figure 3.
Crookes radiometer: force prediction and comparison with experimental data.
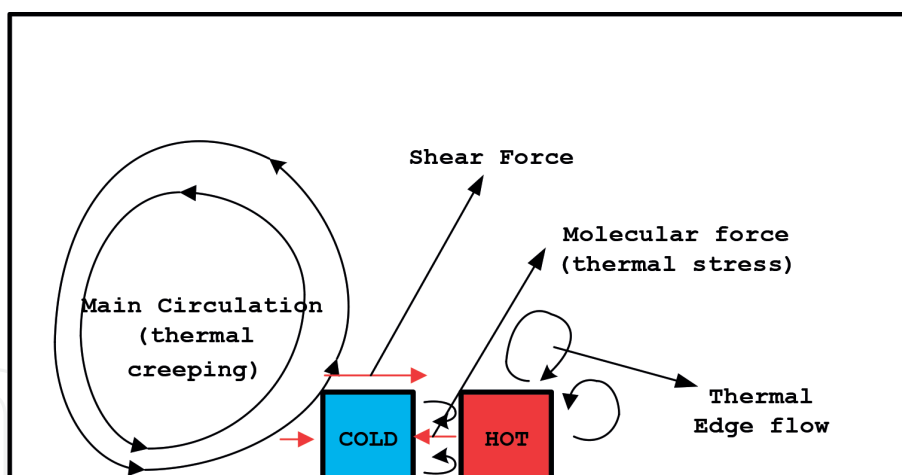
Figure 4.
Flow feature and main stream inside the MIKRA [10].

to equilibrium and the pressures at the centers of two sides of the radiometer are equilibrated, it is not obvious that such an approach is applicable to the regime where the flow is far from equilibrium, and both the area and the edge contribute to the radiometric forces.

The authors of Ref. [47] used an assumption similar to Einstein's, and calculated force with n = 1. They found that the radiometric force computed with this simple empirical expression gives surprisingly close agreement with experimental results, as shown in **Figure 3**. The assumption of n = 1 works very well, even though, the pressure imbalance occurs over a region of 10 mean free paths. The agreement is fairly good in the free molecular and nearly free molecular flows (pressures below or about 0.1 Pa, or Knudsen numbers above 0.5 that are characterized by a nearly linear increase in the radiometric force, and the area-related radiometric forces are dominant). Then, even though the empirical expression stems from the free molecular formula, the agreement is also quite reasonable in the transitional flow where the collisions start to reduce the radiometric force, and both area- and edge-related radiometric forces are important (Knudsen numbers between 0.5 and 0.05, where the maximum radiometric force is observed).

The recognition of the main effective term on this type of sensor is highly significant for the evaluation and performance analysis of this device. According to previous works, three main flow patterns are recognized in this model. As shown in **Figure 4**, the Molecular force Known as thermal stress is the main effective factor that produce the Knudsen force within the gap of two arms. The direction of this force is from hot to cold side. The second dominant term in this model is known as thermal creeping. This flow pattern is produce shear force on the top of cold arm and the direction of this flow is from cold to hot side. The least important flow pattern is thermal edge flow which occurs in the vicinity of the sharp edge with high temperature. In the following, comprehensive details of each factor will be explained.

In the following, the governing equations and the main technical approach for the simulation of this micro gas sensor is presented. In addition, the boundary condition of this model according to the real working condition is defined. Then, the results of various codes are compared to evaluate the performance of each methods. In the next step, the main flow feature inside the model is studied to define the impact of main parameters. Moreover, the effect of the pressure and temperature difference of the hot and cold arm is determined. Finally, the performance of this sensor in detection of gas mixture will be explained.

2. Numerical approach

2.1 Governing equations

In order to simulate the flow inside the rarified gas, Navier-Stokes equations are not valid and consequently, computational fluid dynamics (CFD) approaches is applicable. In fact, the continuity is not governed in low-pressure free molecular regime to near-continuum. Therefore, high order equation of Boltzmann equation should be solved to obtain the flow pattern in molecular regime. In followings, Boltzmann equation is presented.

$$\frac{\partial}{\partial t}(nf) + \mathbf{c}.\frac{\partial}{\partial \mathbf{r}}(nf) + \mathbf{F}.\frac{\partial}{\partial \mathbf{c}}(nf) = Q \tag{4}$$

where n, $\mathbf{c}$, and f are number density, molecular velocity, and velocity distribution function, respectively. In addition, $Q = \int_{-\infty}^{+\infty}\int_0^{4\pi} n^2(f^*f_1^* - ff_1) g \, \sigma \, d\Omega \, d^3 c_1$ is the collision integral which describes the change in the velocity distribution function due to intermolecular collisions.

Since solving the Boltzmann equation is hard, researchers try to find approaches that present similar results to that of Boltzmann equations. DSMC technique of Bird [48], as a particle method based on kinetic theory, is a reliable approach for simulation of rarefied gases. There are some software packages such as OpenFOAM and SPARTA in which DSMC method is developed for the simulation of the engineering problems. OpenFOAM is open-source code is proficient and flexible software for simulation of complex models [49].

2.2 Numerical procedure

In order to perform the DSMC simulations, some assumptions are made. For modeling of the collision, the variable hard sphere (VHS) collision model is used. Collision pairs are chosen based on the no time counter (NTC) method, in which the computational time is proportional to the number of simulator particles [36].

In this type of the sensor, the gap (distance between the heater and shuttle arms) is recognized as the characteristic length (L) and it is 20 μm. In this model, it is recommended to initiate 20 particles in each cell to minimize the statistical scatter.

2.3 Geometry and boundary condition

Figure 5 illustrates the generated grid and the boundary condition applied on the model. The size of the domain is 600 × 300 μm in x and y direction. There were 150 × 65 collision cells in the x and y directions, respectively. All surfaces were assumed to be fully diffuse.

The free domain condition is applied on the top of domain while the side of the domain is symmetry. Constant temperature is applied to the hot and cold arms. The pressure of the domain varied from 0.465 to 11.2 Torr, meaning the Knudsen number varied from 4.64 to 0.19, respectively. The bottom of the domain is at constant temperature (T = 298 K). The simulations are performed for single gas of nitrogen. In this research, two types of the temperature condition (real and constant temperature) are applied on the cold and hot arm. In constant type, it is assumed that the temperature of hot and cold arm is fixed with variation of pressure and effect of four constant temperature differences (310–300, 330–300, 350–300 and 400–300 K) is investigated. In the real temperature type,
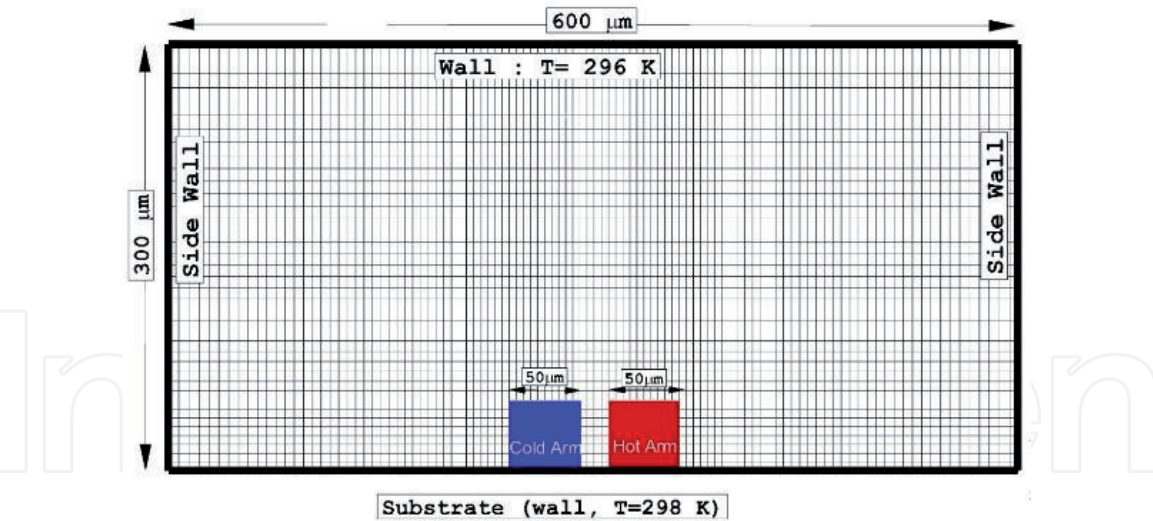
Figure 5.
The boundary condition and grid of the present model [12].

Pressure	Kn	Hot arm	Cold arm
(Pa)	—	(K)	(K)
62	4.48	353	303
155	1.8	350	303
387	0.72	347	303
966	0.29	325	302
1500	0.18	315	300

Table 1.
Temperature of the cold and hot arm (real temperature).

the temperature of the cold and hot arm varies with the pressure of the domain. In order to valid our results, the temperature variation of the cold and hot arm is obtained from experimental data of Strongrich et al. [21] and presented in **Table 1**.

3. Results and discussion

3.1 Verification

In order to evaluate the precision and correctness of the numerical results, it is highly significant to compare simulation with experimental data. As mentioned in the previous section, the results of the SPARTA and DSMC are compared with experimental data (**Figure 6**). The comparison of results of simulations with that of experimental data of Strongrich et al. [21] for various pressure conditions shows that applied assumptions and procedures is logic and reasonable. In addition, obtained results of the SPARTA-DSMC code [21] also confirm the correctness of our results. The evaluation displays a worthy agreement of our work with other techniques.

3.2 Analysis of flow structure

In order to realize the main mechanism of this new gas sensor, the flow feature and temperature distribution inside the micro gas sensor are illustrated in **Figure 7**
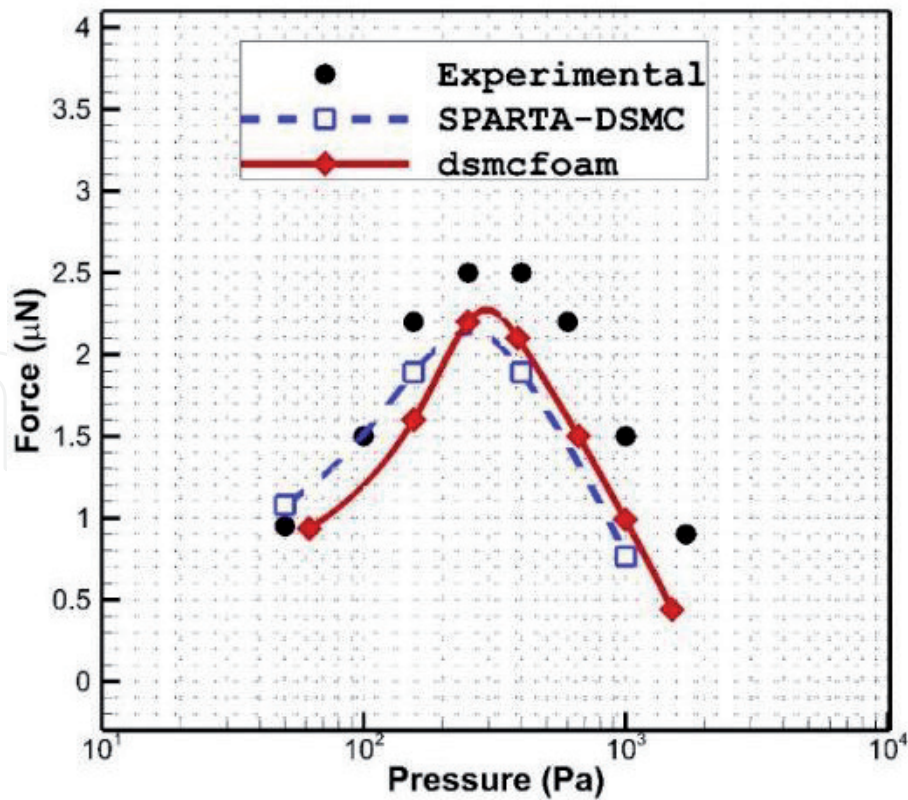
Figure 6.
Comparison of the obtained results (dsmcfoam) with experimental and numerical of Strongrich et al. [21].
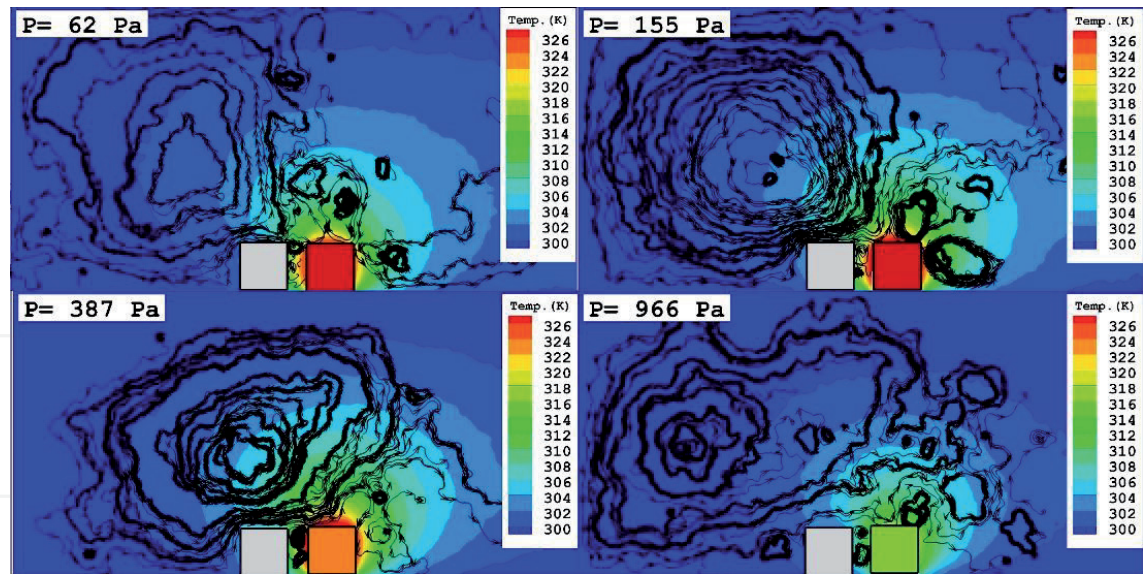

Figure 7.
Flow pattern and temperature distribution inside the MIKRA for different pressure conditions with real arm temperature [11].

when the real temperature is applied on the arms. As shown in the figures, the main characteristics of the flow feature significantly varies with change of the temperature. Since the main difference of flow structure inside the model is related to the temperature distribution, this study also considers the temperature distributions as well as flow pattern.

In low pressure (P = 62 Pa), one big circulation as well as a few small ones are noticed. As the pressure of the domain increases, three main circulations are observed in which two of them is on the top of the hot arm. The main circulation

fully covered the whole domain. It is significant to note that the temperature diffusion strengthen as the pressure of the domain is raised. In high pressure (P = 966 Pa), the temperature of the hot arm is not high enough and the number of the particles considerably increases. Due to these reasons, the diffusion of the temperature inside the domain highly declines. Therefore, the temperature gradient as the main source of the circulation reduces.

3.3 Effect of the temperature difference

As mentioned in the previous section, the effect of the temperature is significant in the performance of this type of micro gas sensor. In order to recognize the main effect of the temperature, constant temperature is applied for all pressure to investigate the effect of pressure (or number of particles) in the performance of the system. **Figure 4** compares the temperature contour along with streamline patterns for various operating pressures when the temperature of the hot and cold arm is fixed 350 and 300 K for all pressure domains, respectively. In this figure, hot arms are colored according to the temperature of particles in the vicinity of arms, while the temperature of the hot solid arm is 350 K. This coloring method improves the perceptibility of the temperature difference in various pressures.

As shown in **Figure 8**, the temperature diffusion to particles that exist in the vicinity of the hot arm increases by raising the pressure of the domain. Indeed, the number of the particles increases when the pressure is raised. Therefore, the particles interaction to hot surface increases in high pressure. The evaluation of the flow feature inside the micro gas sensor will reveal significant results. The main circulation inside domain occurs due to thermal creeping. As the pressure increases inside the model, the main circulation moves to the right side on the top of the gap. Contours clearly show that the strength of the circulation intensifies by growing the pressure till 387 Pa. Then, the circulation weakens inside the domain.

The temperature gradient alters meaningfully from the high pressure (P = 966 Pa) situation to rigorously rarefied (P = 62 Pa) case where noticeable kinks in the contour lines are perceived. These kinks are originated at the sharp angles on the top of the

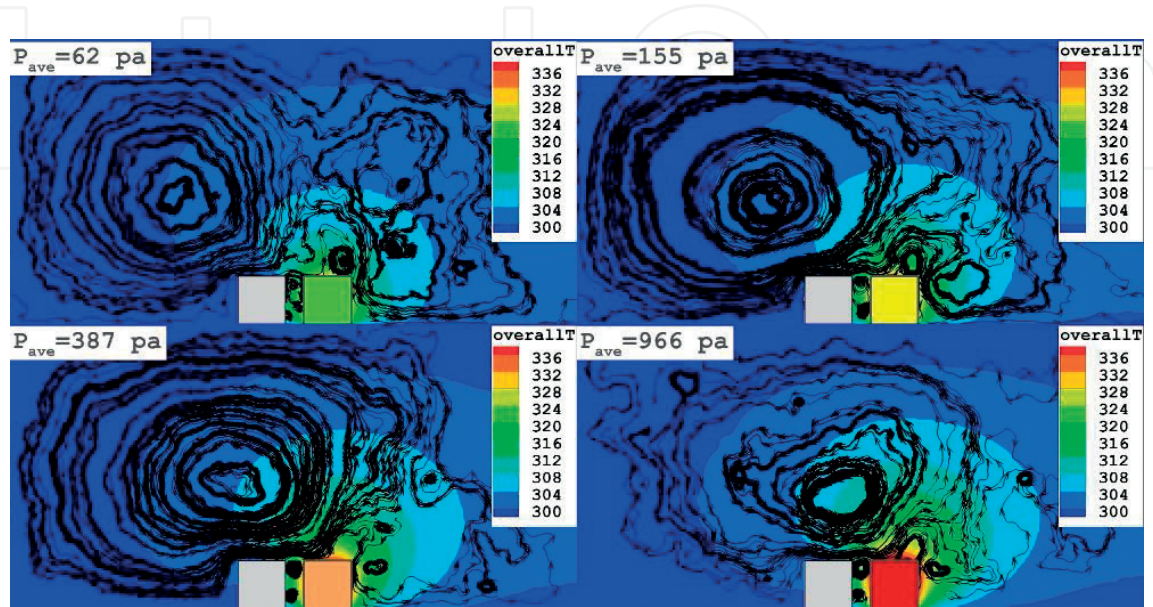**Figure 8.**
Flow pattern and temperature distribution inside the MIKRA for different pressure conditions (T_{hot} = 350, T_{cold} = 300) [10].

arms. Dissimilar to the high-pressure conditions wherein intermolecular collisions promptly smooth out those kinks in the gap of the arms, the absence of adequate intermolecular collisions in the rarefied situations lets these kinks to diffuse much additional away from the hot arms as displayed in **Figure 7**. Therefore, the temperature of hot arm simply enters inside the domain and the noticeable temperature gradient observed in the vicinity of hot arm. In the next sections, it will be clarified how this temperature gradient influences on the induced flow field.

In order to recognize the main impact of the temperature in our problem, **Figure 9** illustrates the flow structure and temperature distribution inside the micro gas sensor in various temperature differences of 10, 30, 50, and 100 K at pressure of 387 Pa. Our findings reveal that the strength of the main circulation intensifies as the temperature difference of the hot and cold arm increases. It was predicted that this would occurs as the temperature gradient inside the model increases. One of important findings of this contour is the temperature penetration. In fact, temperature difference plays significant role on the particles direction. **Figure 10** shows the temperature distribution in the vicinity of the arms. The figure displays that the temperature gradient is intensive on the edges of the hot arm. In order to distinguish the induced flow pattern nearby of the edge, it is supposed that molecules within a mean free path away from
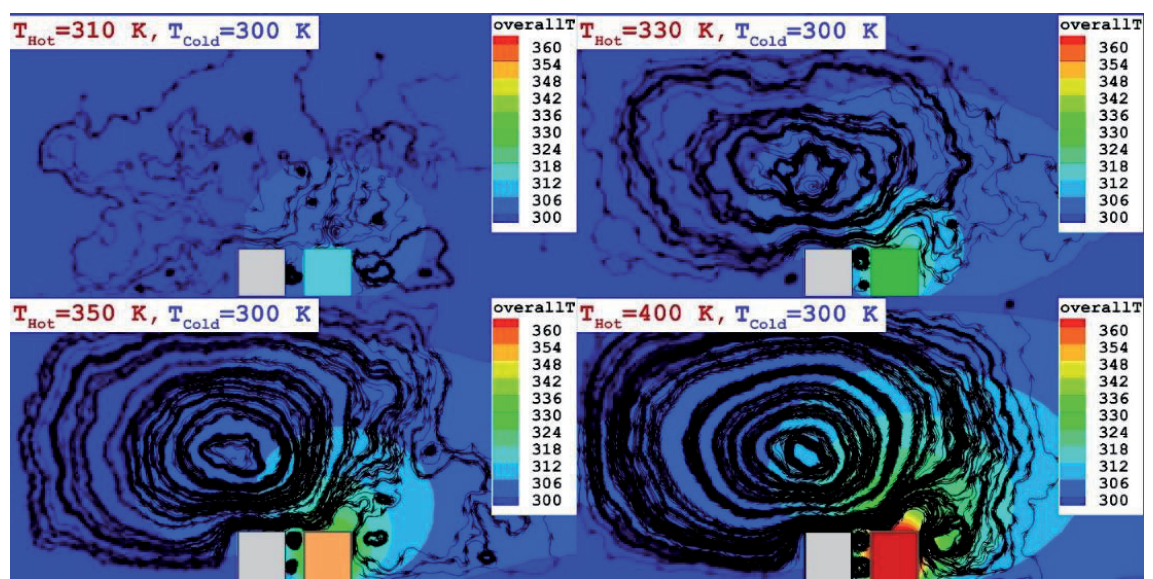

Figure 9.
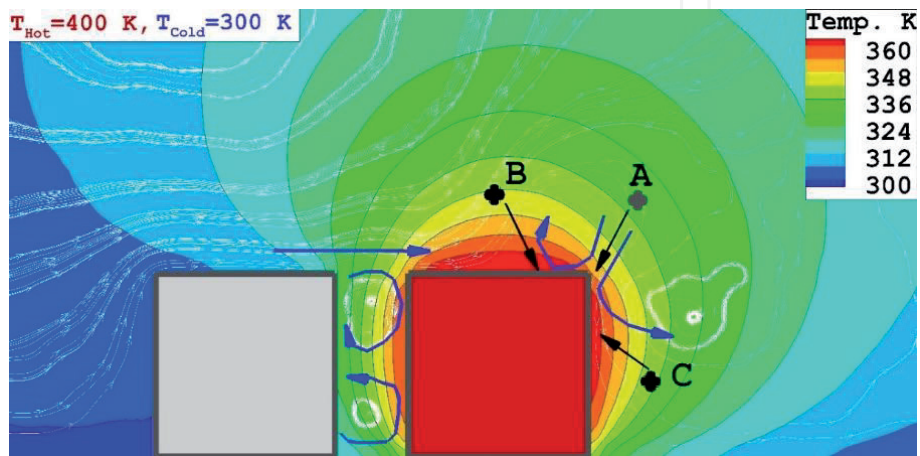*Flow pattern and temperature distribution inside the MIKRA for different temperature differences (P = 387 Pa) [11].*

Figure 10.
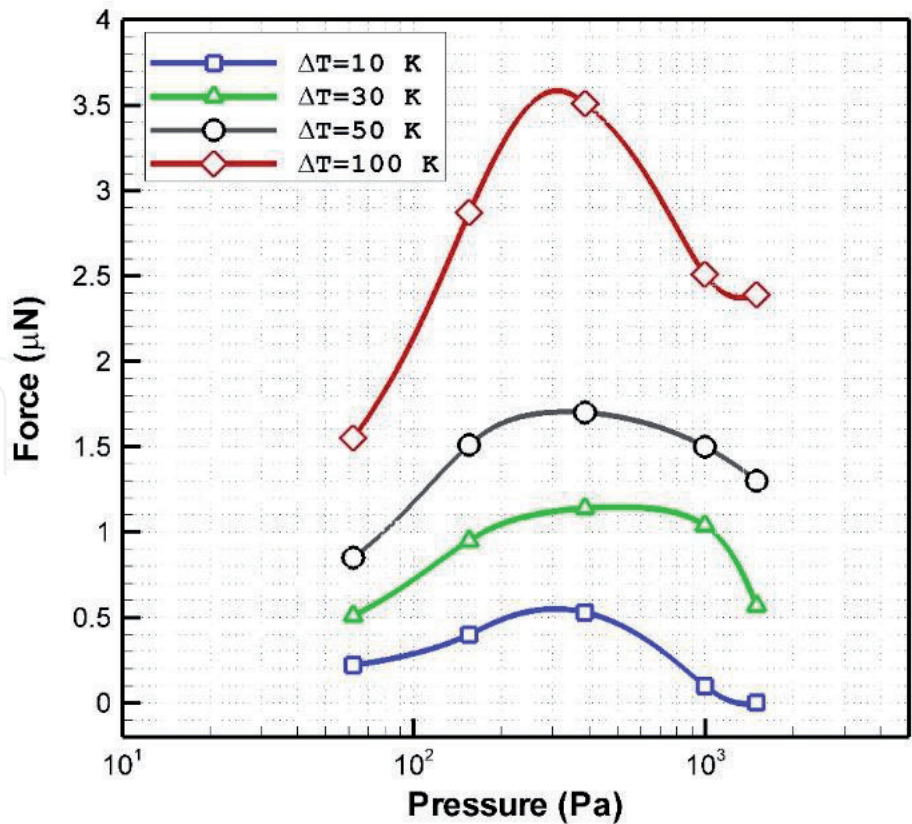*Schematic illustration of the flow feature in the vicinity of the arms [11].*

Figure 11.
Variation of the thermal Knudsen force in various temperature differences [11].

this area arrive at the surface without experiencing any intermolecular collision. As is shown in **Figure 6**, the temperature molecules coming from points B and C is high, while those from point A have low temperatures. Since the diffuse condition is applied as a function of the wall, the tangential velocity of the molecules after collision with the wall is related to the wall temperature. Hence, the tangential velocity of the cold molecules (A) highly increases while hot molecules (B and C) do not experience any change in their velocity. Therefore, the direction of cold molecules after collision is more dominant and they induce a vortex (blue lines) in the edge of the hot arm. Since the temperature of the cold arm is not varied, this flow is not observed on top of the cold arm.

Figure 11 plots the variation of the net force on the cold arm for various temperature differences of 10, 30, 50, and 100 K. Obtained results clearly demonstrate that main inflation occurs in the maximum Knudsen force.

In order to evaluate the primary factors on this micro gas sensor, the effect of force on the both sides of the cold arm is investigated. Since the exerted force should be normalized, Eq. (3) is applied to compare the change of the force as the ratio to exerted force when temperature difference is 10 K.

$$FR = 100 \times \left(\frac{F}{F_{\Delta T=10}} \right)_p. \tag{5}$$

Figure 12 illustrates the variation of the FR for various pressures of domain when the temperature of the hot arm is 30, 50, and 100 K. Comparison of the Knudsen force on both sides of the cold arm clearly reveals that FR declines on right side as the pressure of the domain is increased. This shows that the effect of molecular thermal force within gap is limited due to high interactions of molecules. On the other side, the Knudsen force on the left side of the increases with rising of the pressure of domain. This confirms that the influence of the thermal creeping on the
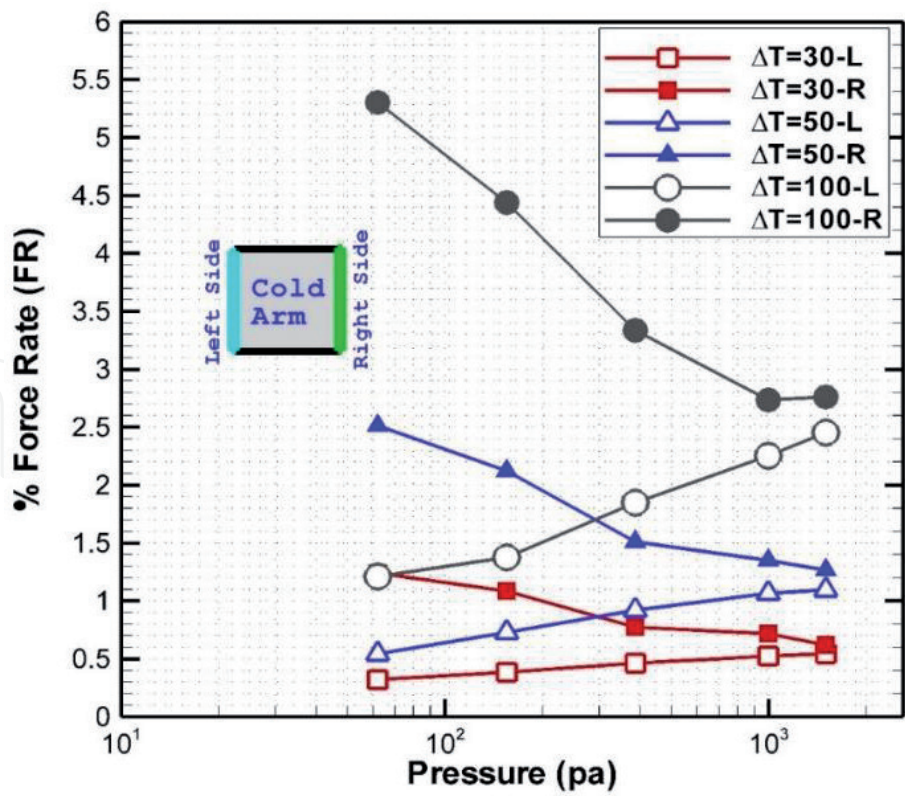
Figure 12.
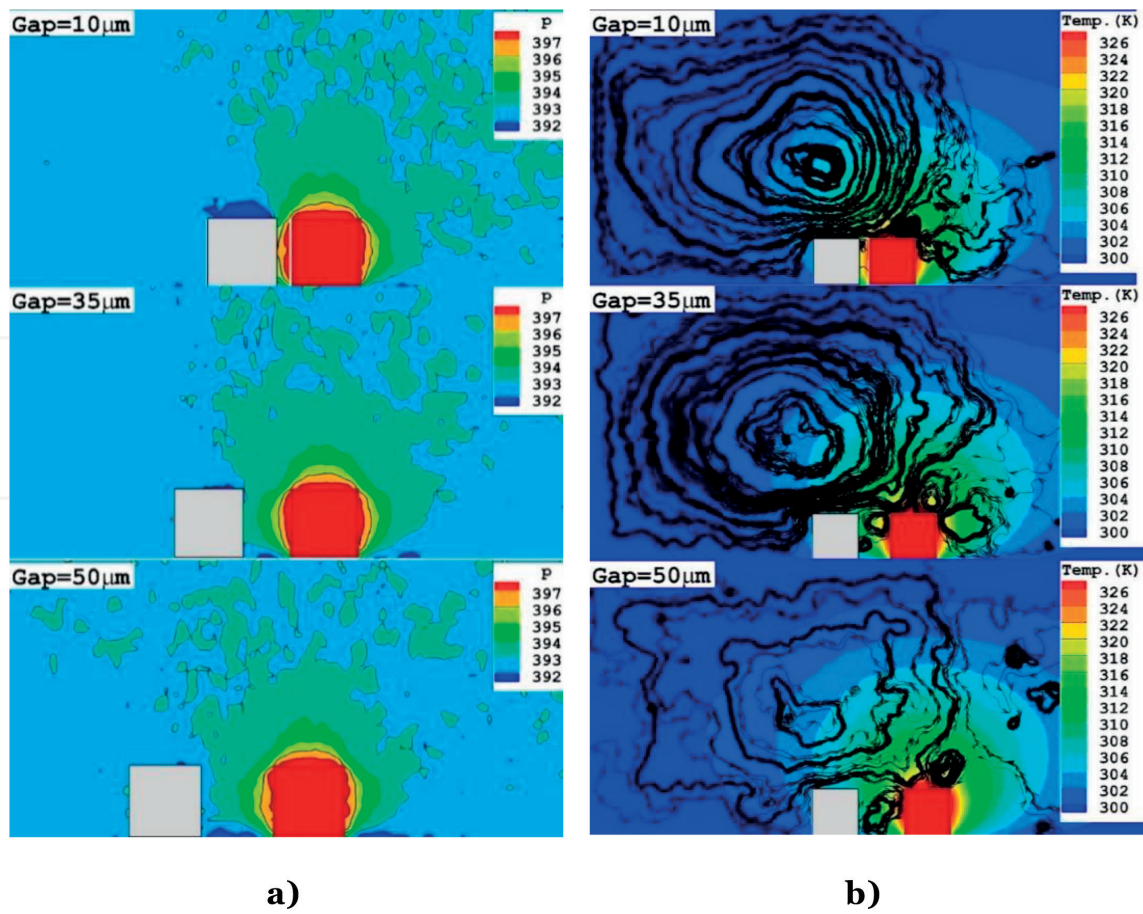*Variation of the exerted force on hot and cold side [11].*

a)   b)

Figure 13.
Comparison of (a) normalized pressure (b) flow pattern and temperature distribution in various gap sizes [12].
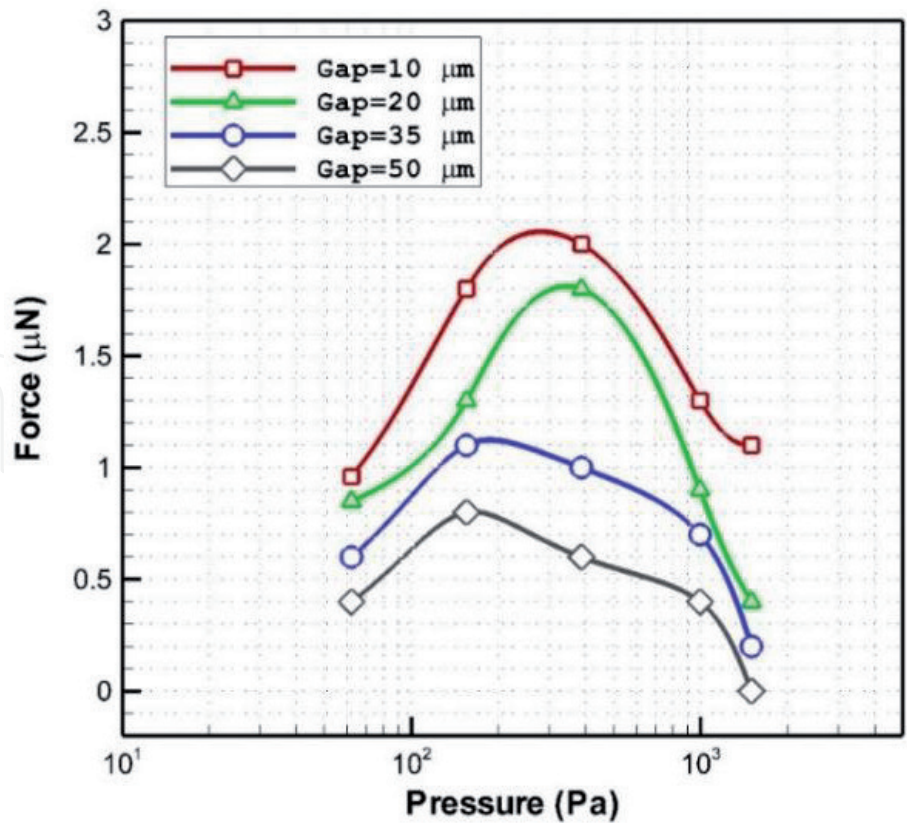
Figure 14.
Comparison of applied Knudsen force on the cold arm for various gap sizes [12].

left side is strengthened. Obtained results also indicate that the rate of FR augments with rising of the temperature difference of the hot and cold arm.

3.4 Effect of gap size

In order to determine the main characteristics of the each term, the pressure of the domain is normalized by the average pressure of domain as follows:

$$I = \frac{P}{P_{ave}}. \tag{6}$$

Since the gap size is crucial in the main characteristics of our problem, the impact of gap size on the normalized pressure and flow structure are depicted in **Figure 13a** and **b**, respectively. As the gap size increases in our model, the thermal creeping effect declines due to high gap of the hot and cold arm. Meanwhile, the number of small circulations increases inside the model.

Figure 14 illustrates the variation of the Knudsen thermal force on the cold arm. Our findings show that increasing the gap size declines the value of the exerted Knudsen force on the model. The variation of the Knudsen force on cold arm presents significant note about the value of the Knudsen number. Since the gap size is known as the specific length (l) in our model, change of this size significantly influence on the value and pressure of the maximum Knudsen force. In low gap size (10 μm), the maximum Knudsen force occurs at 600 Pa while it declines as the gap size is increased to 50 μm. The main impact of gap size on the Knudsen force could be noticed in the pressure distribution. As shown in **Figure 13a**, the pressure gradient hardly reach to the cold arm. This confirms that the pressure gradient is considerably significant on the exerted force.

4. Conclusions

In this study, a DSMC technique is used to investigate rarefied gas inside the low-pressure micro gas sensor. This research has dedicated on the impact of pressure in the flow structure and force generation mechanism. In order to simulate the defined model, Boltzmann equations as governing equations of the present problem are introduced and DSMC method as accessible and robust approach is then offered. The two main key factors are flow patterns and temperature distribution. In this work, these main parameters are compared in various pressures with different temperature of hot and cold arm. Moreover, inclusive physical details on the appliance of Knudsen force production as well as flow structure inside the micro gas actuator are offered. Our findings display that the performance of micro gas sensor highly relies on the temperature difference between hot and cold arms, and the maximum force occurs in specific pressure value for all different temperature difference. On the other side, the effect of gap size is considerable different. Obtained results show that the maximum force occurs in lower pressure as the size of gap is increased. It is also observed that the value of Knudsen force significantly declines when the gap size rises. According to our findings, application of the Knudsen force for the measurement of the gas pressure is a reliable technique and this micro gas actuator could be develop for possible detection of the gas component.

Conflict of interest

There is no conflict of interest in this paper.

Author details

Mostafa Barzegar Gerdroodbary
Department of Mechanical Engineering, Babol Noshirvani University of Technology, Babol, Iran

*Address all correspondence to: mbarzegarg@yahoo.com

IntechOpen

References

[1] Wu CH, Kang D, Chen PH, Tai YC. MEMS thermal flow sensors. Sensors and Actuators A: Physical. 2016;**241**:135-144

[2] Vigne S, Alava T, Videlier H, Mahieu R, Tassetti CM, Duraffourg L, et al. Gas analysis using a MEMS linear time-of-flight mass spectrometer. International Journal of Mass Spectrometry. 2017;**422**:170-176

[3] Mirzaei M, Poozesh A. Simulation of fluid flow in a body-fitted grid system using the lattice Boltzmann method. Physical Review E. 2013;**87**(6):063312

[4] Verma VK, Yadava RD. Stochastic resonance in MEMS capacitive sensors. Sensors and Actuators B: Chemical. 2016;**235**:583-602

[5] Grzebyk T, Górecka-Drzazga A. MEMS type ionization vacuum sensor. Sensors and Actuators A: Physical. 2016;**246**:148-155

[6] Gerdroodbary MB, Ganji DD, Taeibi-Rahni M, Pruiti B, Moradi R. Development of Knudsen thermal force for mass analysis of CH4/He gas mixture. International Journal of Modern Physics C. 2019;**30**(01):1-16

[7] Sarabi S, Bogy DB. Effect of functional end-groups on lubricant reflow in heat-assisted magnetic recording (hamr). Tribology Letters. 2017;**65**(1):15

[8] Mahyari A, Barzegar Gerdroodbary M, Mosavat M, Ganji DD. Detection of ammonia gas by Knudsen thermal force in micro gas actuator. Case Studies in Thermal Engineering. 2018;**12**:276-284

[9] Barzegar Gerdroodbary M, Ganji DD, Moradi R, Abdollahi A. Application of Knudsen thermal force for detection of CO2 in low-pressure micro gas sensor. Fluid Dynamics. 2018;**53**(6):795-806

[10] Gerdroodbary MB, Ganji DD, Taeibi-Rahni M, Vakilipour S, Moradi R. Application of direct simulation Monte Carlo for development of micro gas sensor. Bulgarian Chemical Communications. 2018;**50**(2):298-305

[11] Gerdroodbary MB, Ganji DD, Taeibi-Rahni M, Vakilipour S. Effect of Knudsen thermal force on the performance of low-pressure micro gas sensor. The European Physical Journal Plus. 2017;**132**(7):315

[12] Gerdroodbary MB, Ganji DD, Taeibi-Rahni M, Vakilipour S. Effect of geometrical parameters on radiometric force in low-pressure MEMS gas actuator. Microsystem Technologies. 2018;**24**(5):2189-2198

[13] Gerdroodbary MB, Anazadehsayed A, Hassanvand A, Moradi R. Calibration of low-pressure MEMS gas sensor for detection of hydrogen gas. International Journal of Hydrogen Energy. 2018;**43**(11):5770-5782

[14] Gerdroodbary MB, Mosavat M, Ganji DD, Taeibi-Rahni M, Moradi R. Application of molecular force for mass analysis of krypton/xenon mixture in low-pressure MEMS gas sensor. Vacuum. 2018;**150**:207-215

[15] Gerdroodbary MB, Ganji DD, Shiryanpour I, Moradi R. Mass analysis of CH$_4$/SO$_2$ gas mixture by low-pressure MEMS gas sensor. Journal of Natural Gas Science and Engineering. 2018;**53**:317-328

[16] Hassanvand A, Gerdroodbary MB, Moradi R, Amini Y. Application of Knudsen thermal force for detection of inert gases. Results in Physics. 2018;**9**:351-358

[17] Ketsdever A, Gimelshein N, Gimelshein S, Selden N. Radiometric phenomena: From the 19th to the 21st century. Vacuum. 2012;**86**(11):1644-1662

[18] Crookes W. On attraction and repulsion resulting from radiation. Philosophical Transactions of the Royal society of London. 1874;**164**:501-527

[19] Strongrich AD, O'Neill WJ, Cofer AG, Alexeenko AA. Experimental measurements and numerical simulations of the Knudsen force on a non-uniformly heated beam. Vacuum. 2014;**109**:405-416

[20] Strongrich A, Alexeenko A. Microstructure actuation and gas sensing by the Knudsen thermal force. Applied Physics Letters. 2015;**107**:193508

[21] Strongrich AD, Pikus AJ, Sebastiao IB, Peroulis D, Alexeenko AA. Low-pressure gas sensor exploiting the knudsen thermal force: Dsmc modeling and experimental validation. In: 2016 IEEE 29th International Conference on Micro Electro Mechanical Systems (MEMS) (IEEE, 2016). pp. 828-831

[22] Passian A, Warmack RJ, Ferrell TL, Thundat T. Thermal transpiration at the microscale: A Crookes cantilever. Physical Review Letters. 2003;**90**(12):124503

[23] Passian A, Wig A, Meriaudeau F, Ferrell TL, Thundat T. Knudsen forces on microcantilevers. Journal of Applied Physics. 2002;**92**(10):6326-6333

[24] Passian A, Warmack RJ, Wig A, Farahi RH, Meriaudeau F, Ferrell TL, et al. Observation of Knudsen effect with microcantilevers. Ultramicroscopy. 2003;**97**(1):401-406

[25] Lereu AL, Passian A, Warmack RJ, Ferrell TL, Thundat T. Effect of thermal variations on the Knudsen forces in the transitional regime. Applied Physics Letters. 2004;**84**(6):1013-1015

[26] Sista SV, Bhattacharya E. Knudsen force based MEMS structures. Journal of Micromechanics and Microengineering. 2014;**24**:045003

[27] Kaajakari V, Lal A. Thermokinetic actuation for batch assembly of microscale hinged structures. Journal of Microelectromechanical Systems. 2003;**12**:425-432

[28] Aoki K, Sone Y, Yano T. Numerical analysis of a flow induced in a rarefied gas between noncoaxial circular cylinders with different temperatures for the entire range of the Knudsen number. Physics of Fluids A: Fluid Dynamics. 1989;**1**(2):409-419

[29] Zhu T, Ye W. Origin of Knudsen forces on heated microbeams. Physical Review E. 2010;**82**:036308

[30] McNamara S, Gianchandani YB. On-chip vacuum generated by a micromachined Knudsen pump. Journal of Microelectromechanical Systems. 2005;**14**:741

[31] Sarabi S, Bogy DB. Effect of viscoelasticity on lubricant behavior under heat-assisted magnetic recording conditions. Tribology Letters. 2018;**66**(1):33

[32] Sarabi MS, Bogy DB. Simulation of the performance of various PFPE lubricants under heat assisted magnetic recording conditions. Tribology Letters. 2014;**56**(2):293-304

[33] Sheikholeslami M, Gerdroodbary MB, Moradi R, Shafee A, Li Z. Application of neural network for estimation of heat transfer treatment of Al_2O_3-H_2O nanofluid through a channel. Computer Methods in Applied Mechanics and Engineering. 2019;**344**:1-12

[34] Fallah K, Gerdroodbary MB, Ghaderi A, Alinejad J. The influence of micro air jets on mixing augmentation of fuel in cavity flameholder at supersonic flow. Aerospace Science and Technology. 2018;**76**:187-193

[35] Gerdroodbary MB, Imani M, Ganji DD. Investigation of film cooling on nose cone by a forward facing array of micro-jets in hypersonic flow. International Communications in Heat and Mass Transfer. 2015;**64**:42-49

[36] Moradi R, Mosavat M, Barzegar Gerdroodbary M, Abdollahi A, Amini Y. The influence of coolant jet direction on heat reduction on the nose cone with Aerodome at supersonic flow. Acta Astronautica. 2018;**151**:487-493

[37] Gerdroodbary MB, Imani M, Ganji DD. Heat reduction using conterflowing jet for a nose cone with Aerodisk in hypersonic flow. Aerospace Science and Technology. 2014;**39**:652-665

[38] Hassanvand A, Barzegar Gerdroodbary M, Fallah K, Moradi R. Effect of dual micro fuel jets on mixing performance of hydrogen in cavity flameholder at supersonic flow. International Journal of Hydrogen Energy. 2018;**43**(20):9829-9837

[39] Barzegar Gerdroodbary M, Younes Amini DD, Ganji MRT. The flow feature of transverse hydrogen jet in presence of micro air jets in supersonic flow. Advances in Space Research. 2017;**59**:1330-1340

[40] Gerdroodbary MB, Sheikholeslami M, Valiallah Mousavi S, Anazadehsayed A, Moradi R. The influence of non-uniform magnetic field on heat transfer intensification of ferrofluid inside a T-junction. Chemical Engineering and Processing-Process Intensification. 2018;**123**:58-66

[41] Vo DD, Moradi R, Gerdroodbary MB, Ganji DD. Measurement of low-pressure Knudsen force with deflection approximation for gas detection. Results in Physics. 2019;**30**(1):1-16

[42] Epstein PS. Theorie des radiometers. Zeitschrift für Physik. 1929;**54**:537-563

[43] Einstein A. Zur theorie der radiometrerkrafte. Zeitschrift für Physik. 1924;**27**:1-5

[44] Schuster A. On the nature of the force producing the motion of a body exposed to rays of heat and light. Proceedings. Royal Society of London. 1875;**24**:391-392

[45] Brüche E, Littwin W. Experimental contributions to the radiometer question. Zeitschrift für Physik. 1928;**52**:318-335

[46] Scandurra M, Iacopetti F, Colona P. Gas kinetic forces on thin plates in the presence of thermal gradients. Physical Review E. 2007;**75**:026308

[47] Selden N, Ngalande C, Gimelshein N, Gimelshein S, Ketsdever A. Origins of radiometric forces on a circular vane with a temperature gradient. Journal of Fluid Mechanics. 2009;**634**:419-431

[48] Bird GA. Molecular Gas Dynamics and the Direct Simulation of Gas Flows. Oxford: Clarendon Press; 1994

[49] OpenFOAM: The Open Source CFD Toolbox, User Guide, Version 1.6. 2009